JOURNAL OF CATALYSIS **169,** 287–300 (1997)
ARTICLE NO. CA971640

Characterization of $AgMo_3P_2O_{14}$ Catalyst Active in Propane Mild Oxidation

L. Savary,* G. Costentin,*,[1] F. Maugé,* J. C. Lavalley,* J. El Fallah,† F. Studer,‡ A. Guesdon,‡ and H. Ponceblanc§

*Laboratoire de Catalyse et Spectrochimie, Institut des Sciences de la Matière et de Rayonnement, 6 Bd du Maréchal Juin, 14050 Caen Cedex, France; †Laboratoire Universiteire des Sciences Appliquées de Cherbourg, Site Universitaire, B.P. 78, 50130 Octeville, France; ‡Laboratoire de Cristellogrephie et Science des Materieaux, Institut des Sciences de la Mastière et de Rayonnement, 6 Bd du Maréchal Juin, 14050 Caen Cedex, France; and §Rhône-Poulenc Recherches, 52 rue de la Haie Coq, 93308 Aubervilliers Cedex, France

Received October 28, 1996; revised January 15, 1997; accepted January 15, 1997

A new silver molybdenum phosphate, $AgMo_3P_2O_{14}$, involving a mixed molybdenum valency, was found to play a role in mild propane oxidation (6% propane conversion, 70% propene selectivity, 6% acrolein selectivity at 733 K). Comparisons with results obtained with other molybdenum phosphates showed that silver presented a positive influence when it was able to migrate inside the MoPO host lattice. Characterizations of this catalyst, by XRD, X-ray absorption spectroscopy, and XPS, performed before and after catalytic tests, emphasized the importance of the redox couple Mo^V/Mo^{VI}. Moreover, the ability of the framework to allow the establishment of a correct Mo^V/Mo^{VI} balance of 2/1 was found to be a determining factor.

INTRODUCTION

The selective oxidation of alkanes into useful chemical compounds is becoming increasingly important, from both fundamental and industrial points of view. In fact, the cost of propane feedstock is about five to six times less than the cost of propene. Thus, the two main technological options for producing acrolein are based on propane as the main material:

—a two-stage process based on a first dehydrogenation step of propane to propene followed by a conventional unit for propene oxidation to acrolein, which is currently the commercially available process.

—a direct one-stage propane conversion to acrolein which appears, economically, to be an attractive alternative.

Nevertheless, the latter solution is accompanied by many difficulties due to the low reactivity of propane compared to that of propene and formed oxygenated products. Developments in this subject would suggest the employment of bifunctional catalysts. But little has been reported on the partial oxidation of propane (1–11).

Since the selective oxidation of *n*-butane to maleic anhydride has been successfully established using VPO catalysts (12–14), this system has also been investigated for mild propane oxidation (15–22). Other studies have also been carried out in order to develop multicomponent oxide catalysts such as BiMoO, BiMoVAgO, BiBaTeO, and BPO systems (1–6). In particular, Moro-Oka and co-workers (2) reported that an Ag-doped bismuth vanadomolybdate catalyst with a scheelite structure was selective to acrolein and acrylonitrile.

One of the main characteristics of oxidation reactions is that they are structure-sensitive. We attempted to study the relationships between the structure and the composition of well-defined original compounds, here molybdenum phosphates in various Mo oxidation states with their catalytic properties. In this paper, we investigate the catalytic behavior of molybdenum phosphates, involving silver as the inserted cation, or not, for propane mild oxidation. The compounds display different new formulations, $AgMo_3P_2O_{14}$ (23), $SrMo_3P_2O_{14}$ (23), $AgMoPO_6$ (24), $AgMo_5P_8O_{33}$ (25), $NaMo_5P_8O_{33}$, and $Ag_{0.5}Na_{0.5}Mo_5P_8O_{33}$, and offer the opportunity for well-defined active centers in ordered matrices which had previously been characterized by XRD. The influence of silver in several host lattices with different Mo reduction states is appreciated. Different catalyst characterizations (XRD, EXAFS, XANES, and XPS) performed before and after reaction allow one to specify the possibility of eventual modifications during reaction.

EXPERIMENTAL

Preparation of the Catalysts

Preparation methods for $AgMo_3P_2O_{14}$, $SrMo_3P_2O_{14}$, $AgMoPO_6$, $NaMo_5P_8O_{33}$, and $AgMo_5P_8O_{33}$ phases have

[1] To whom correspondence should be addressed. Fax: 31452822. E-mail: LAVALLEY@ISMRA.UNICAEN.FR.

0021-9517/97 $25.00

TABLE 1

Prepared Phases

Final prepared phase	Average oxidation state for molybdenum atoms	First step intermediate product	Temperature of the second step (K)
$AgMo_3P_2O_{14}$	5.66	$AgMo_{2.83}P_2O_{14}$	873
$SrMo_3P_2O_{14}$	5.33	$SrMo_{2.667}P_2O_{14}$	1023
$AgMoPO_6$	6	$AgMoPO_6$	923
$AgMo_5P_8O_{33}$	5	$AgMo_{4.167}P_8O_{33}$	1123
$Ag_{0.5}Na_{0.5}Mo_5P_8O_{33}$	5	$Ag_{0.5}Na_{0.5}Mo_{4.167}P_8O_{33}$	1123
$NaMo_5P_8O_{33}$	5	$NaMo_{4.167}P_8O_{33}$	1123

already been described in the literature (23–25). We have extended them to the synthesis of the $Ag_{0.5}Na_{0.5}Mo_5P_8O_{33}$ compound.

All the compounds described in this paper, except $AgMoPO_6$, involve molybdenum in a reduced oxidation state. The formal molybdenum oxidation states in the phases studied are reported in Table 1. To prepare such materials two steps were necessary. First, $(NH_4)_2HPO_4$, MoO_3, and A_2CO_3 (A = Ag, Na) or $SrCO_3$ were mixed in an agate mortar in a ratio adequate for obtaining intermediate compounds involving molybdenum species with VI valency. The formulations of these intermediate compounds, which are given in Table 1, were therefore substoichiometric in molybdenum compared to the final products. The various mixtures were heated at about 673 K in air (873 K in the case of the strontium compound), in a platinum crucible, for at least 3 h in order to eliminate CO_2, NH_3, and H_2O. In a second step, the finely ground products were mixed with an appropriate amount of metallic molybdenum to allow reduction of molybdenum Mo^{VI} to the above-mentioned values (Table 1). The mixtures were heated in evacuated silica tubes for 6 h at different temperatures according to the nature of the prepared phase (Table 1).

Catalytic Tests

Reaction Procedure

The catalytic tests were carried out in a fixed-bed continuous-flow quartz microreactor (capillary U tube, i.d. 2 mm), under atmospheric pressure, in the temperature range from 573 to 723 K. The catalyst loading was made of 1 g of granules in the size range of 0.16–0.3 mm. To minimize possible homogeneous reactions, the volume was reduced as far as possible by filling the reactor before and after the catalytic bed with quartz powder. It was also checked, by using a reactor filled with quartz powder instead of catalyst, that there was no significant catalytic contribution from the glass walls of the reactor and that the homogeneous reaction could be neglected. The temperature of the catalyst bed was maintained within ± 1 K of the required value, controlled by a thermocouple located close to the wall of the quartz tube. In each case, the catalyst was heated to 573 K in the stream of reactants, and this temperature was held for 2 h. The temperature was then gradually raised to 623, 673, and 723 K, each temperature being held for about 1 h. The catalytic activity analyses were successively performed at 45-min intervals. The feed was a C_3H_8–O_2 mixture diluted with N_2, with a $C_3H_8/O_2/N_2$ molar composition of 60/20/20. The total flow rate was 8 ml/min to realize a W/F of 3.5 g · h · liter^{-1}, which corresponds to a contact time T_c of above 8 s.

For the study of $AgMo_3P_2O_{14}$ activity as a function of contact time, the reactive flows were adjusted to correct values to obtain a contact time ranging from $T_c = 0.15$ to 10 s.

Analyses

The reactor inlet and outlet gases were analyzed on line by gas chromatography. The tube connecting the reactor to the chromatographs was heated at 453 K in order to avoid any condensation of reaction products. The analyses were performed on line by means of two chromatographs in series: a Hewlett Packard HP 5890 gas chromatograph equipped with two parallel detectors [a flame ionization detector (FID) and a thermal conductivity detector (TCD)] and a Varian chromatograph equipped with a TCD. In fact, the gases entering and leaving the reactor passed through a sampling system involving two gas valves: a 10-way valve fed the reactants or effluent gases to the two parallel detectors of the HP chromatograph and to a 6-way valve, situated at the exit of the previous one, which fed the gases to the third detector (Varian). The injection valves were actuated automatically by means of an HP 3396 integrator.

Separation of organic oxygenated compounds was performed on a CPSIL column (50 m, i.d. 0.32 mm). A suitable separation of O_2, N_2, CO, and CO_2 was achieved by using the two TCD detectors: (i) O_2, N_2, and CO were separated on a molecular sieve 5A column (4 m, i.d. 2.2 mm) connected to the HP TCD detector; (ii) (air + CO), CO_2, and propene were analyzed by means of two packed columns in series: a Hayesep Q (3 m, i.d. 2.2 mm, $T = 353$ K) and a Hayesep DB (2 m, i.d. 2.2 mm, $T = 353$ K) connected to the Varian TCD detector. Each analysis was about 45 min long, and a temperature program was required to analyze the products separated on the HP chromatograph: the temperature was maintained at 313 K for 30 min, and then was raised to 353 K (40 K/min).

In the following discussion, conversions and selectivities are defined as follows:

$$\text{conversion in propane} = \frac{\text{summation of moles of all formed products}}{\text{moles of propane initially present}}$$

$$\text{selectivity in product } X = \frac{\text{moles of } X \text{ product formed}}{\text{summation of moles of all formed products}} \times \frac{\text{number of carbons in } X \text{ product}}{3}.$$

This analytic procedure was found to be effective, as the carbon balance was very close to 1. The activity measurements were performed several times for each catalyst and for each temperature. Their reproducibility allowed us to be confident of the results, even those obtained at low conversion.

Characterization Methods

XRD

X-ray diffraction patterns of $AgMo_3P_2O_{14}$, $SrMo_3P_2O_{14}$, $AgMoPO_6$, and $AgMo_3P_5O_{33}$ samples were indexed following the crystallographic symmetries and parameters deduced from the single-crystal studies (23–25). The isotypy of $Ag_{0.5}Na_{0.5}Mo_5P_8O_{33}$ and $NaMo_5P_8O_{33}$ with $AgMo_3P_5O_{33}$ was also checked by indexing their X-ray powder diffraction using the crystallographic parameters of $AgMo_3P_5O_{33}$. These characterizations ensured that samples were single phase and very well crystallized but therefore implied very low specific areas for all samples (<1 m^2/g).

No modification of X-ray powder diffraction patterns was detected after catalytic tests.

X-Ray Absorption Measurements

X-ray absorption measurements were carried out at the French Synchrotron Laboratory LURE, using the DCI storage ring and EXAFS IV beamline equipped with a two-crystal Si (311) monochromator. During the experiments, the storage ring using 1.85 GeV positrons with average intensity 250 mA.

Data were collected in transmission mode chambers at room temperature.

Samples were pressed into pellets of absorbance close to 1 above the Mo *K*-edge. EXAFS Mo *K*-edge (19,999 eV) spectra were taken at room temperature with 2-eV steps in the energy range 19,900–20,700 eV. Threshold spectra were recorded in the range 19,950–20,100 eV, with 1-eV steps and a measuring time of 2 s per data point.

XANES Data Processing

The normalization procedure used throughout this work was a standard one: after subtraction of the same diffusion background from the XANES and EXAFS spectra, recorded under the same experimental conditions, a point at high energy where no more EXAFS oscillations were still observable was set to unity. Then the intensity of a point with an energy between 50 and 100 eV from the edge was recorded on the EXAFS spectrum and was reported on the XANES to set the normalized height.

EXAFS Data Processing

The EXAFS analysis was performed following a well-known procedure (26, 27), through a chain of programs written by Michalowicz (28). The absorption spectra studied were obtained by summing two experimental spectra recorded under the same conditions $\mu(E) = \ln(\Sigma I_0/\Sigma I)$. The EXAFS signal $\mu(E)$ is equal to $[\mu(E) - \mu_1(E)]/[\mu_1(E) - \mu_0(E)]$, where $\mu(E)$ is the observed absorption, $\mu_1(E)$ the atomic absorption, and $\mu_0(E)$ the sample absorption. This last parameter was deduced from an analytical expression using the formula of Lengeler and Eisenberg (29). The atomic absorption coefficient $\mu_1(E)$ was approximated by a fourth-degree polynomial expression from 20,036 to 20,690 eV. The EXAFS contribution was calculated between 20,044 and 20,690 eV with, E_0 taken equal to the energy at half the edge jump, 20,007 eV. The EXAFS spectra multiplied by a cubic k factor were then Fourier transformed (FT) in the k 3.3 to 12.4 Å^{-1} range after application of a KAISER window ($\tau = 2.5$). After FT, the contribution of each atomic shell surrounding the absorbing atom Mo could be isolated in the R space. The positions R' where the peaks appear were lower than the true distances to the corresponding scatterers (by displacements of 0.3–0.5 Å) because FTs were obtained without correction for the backscattering phase and amplitude functions. Theoretical backscattering phase and amplitude were then used (30) and the positional agreement between the calculated structure and the experimental data was quite good.

A fitting procedure with simplex and gradient methods using the MINUIT program (31) was applied. For all the fits, the number of variables was chosen so as not to pass beyond $(N_{\text{ind}} - 1)$, with N_{ind} defined as the number of independent variables and equal to $2\Delta k \Delta R/\Pi$, where $\Delta k = \Delta k_{\max} - \Delta k_{\min}$ and ΔR is the size of the back-Fourier-transformed window.

$$k\chi(k) = -S_0^2 \sum_i N_i/R_i^2 \exp\left(-2k^2\sigma_i^2\right) \times \exp(-2R_i\Gamma/k)\, f_i(\Pi, k) \sin[2kR_i + \Phi_i(k)],$$

where S_0 is the scale factor (just a fraction of the photoelectrons ejected are taking part in the EXAFS phenomenon); N_i is the number of neighbors at a distance R_i from the absorbing atom; $\Gamma = k/\lambda$, where λ is the mean free path of the photoelectron; $f_i(\Pi, k)$ and $\Phi_i(k)$ are respectively the amplitude and phase shift functions characteristic of the ejection of the electron from the central atom and its backscattering by the neighbors; and σ_i is a damping coefficient due to thermal motion and distance distribution in the shell, i.e., the Debye–Waller factor. When theoretical amplitude and phase shift are used, S_0 and Γ can be considered agreement

factors. Therefore, they are not allowed to vary for the entire series of samples.

XPS Measurements

The XPS analyses were performed in a Riber system equipped with a hemispherical analyzer (Leybold). The residual pressure in the spectrometer was in the range 7×10^{-7} to 7×10^{-8} Pa. The source was the $K\alpha$ ray of a Mg anode (10 mA–13 kV). The pass energy of the analyzer was constant and tuned at 50 meV. The spectra were scanned with 50-meV steps for 50 ms for each step. No flood gun was used.

The integral intensities of the most intense peaks of each element were measured after subtraction of the satellite peaks and subtraction of the Shirley type background.

The samples were introduced into the spectrometer without *in situ* thermal treatment and were outgassed overnight; the C_{1s} peak was too broad to be used for binding energy calibration. The P_{2p} peak, for which the oxidation state was constant whatever the sample, appeared to be a more accurate internal reference. The charge correction was done by fitting the binding energy of P_{2p} at 135.0 eV.

RESULTS AND DISCUSSION

Reactivity Results

$AgMo_3P_2O_{14}$ and $SrMo_3P_2O_{14}$

First, the catalytic performances for propane partial oxidation of the $AMo_3P_2O_{14}$ (A = Ag, Sr) system were studied. Conversion variations were achieved by varying the inlet temperature between 573 and 733 K. The main results in terms of C_3H_8 and O_2 conversions and selectivities which were obtained on the two samples between 623 and 733 K are reported in Table 2. It appears that although $AgMo_3P_2O_{14}$ is less active than $SrMo_3P_2O_{14}$, it is more selective in mild oxidation products than the latter. The major organic product was propene; acrolein, propanal, and acetic acid were also formed as minor products. The increase of conversion with temperature is more pronounced in the case of $SrMo_3P_2O_{14}$, whose propane conversion reaches 11.5% versus 7% in the case of $AgMo_3P_2O_{14}$.

The selectivity in propene reaches a maximum for $AgMo_3P_2O_{14}$ (82%) at 683 K and then decreases to 70% at 733 K, whereas in the case of the $SrMo_3P_2O_{14}$ compound, it decreases with increasing temperature to reach 35% at 733 K.

The selectivity in acrolein is low in the two cases, but the variations with temperature are once again different: it increases with temperature for $AgMo_3P_2O_{14}$ (6% at 733 K), whereas it is quite independent of temperature for $SrMo_3P_2O_{14}$ (~2%). Propanal and acetic acid are formed in low proportions.

TABLE 2

Catalytic Results Obtained on $AgMo_3P_2O_{14}$ and $SrMo_3P_2O_{14}$ Samples for Propane Mild Oxidation between 623 and 733 K

	Temp (K)	$AgMo_3P_2O_{14}$	$SrMo_3P_2O_{14}$
Propane conversion (%)	623	1	1.5
	683	3	5
	733	7	11.5
Selectivity in propene (%)	623	80	77
	683	82	42
	733	70	35
Selectivity in acrolein (%)	623	2	3
	683	4	2
	733	6	2
Selectivity in propanal (%)	623	3	5
	683	2	4
	733	1	3
Selectivity in acetic acid (%)	623	0	2
	683	2	1
	733	2	0
Selectivity in CO_2 (%)	623	15	13
	683	6	8
	733	8	16
Selectivity in CO (%)	623	0	0
	683	1	41
	733	10	43

As far as CO_x selectivity is concerned, at low temperature (623 K) the two solids exhibit almost the same CO_2 selectivity, whereas at or above 683 K the CO_x selectivity of $SrMo_3P_2O_{14}$ is much higher than that of $AgMo_3P_2O_{14}$ (59% versus 18% at 733 K), the main difference resulting from CO selectivity (41% versus 1% at 683 K). The balance is propene selectivity. More precisely, as temperature increases to 733 K, CO_2 formation increases because of secondary oxidation reactions, as shown by its yield values (Y_{CO_2} = 0.15, 0.18 and 0.56% at respectively 623, 683, and 733 K). Nevertheless, for both compounds, at above 683 K, CO_2 reaches a minimum of selectivity. We can note that this temperature corresponds to the appearance of CO, which is a high-temperature product, in high quantity. This thus results in a decrease in CO_2 selectivity.

The fact that CO_2 selectivity is higher at 623 K than at 683 K could also indicate that it is partially a primary product. This result is confirmed by the study of the variation of the selectivities as a function of contact time: activity was measured at several contact times (0.15 to 10 s) by varying the reactive flow with $C_3H_8/O_2/N_2 = 60/20/20$ and $T = 733$ K. As expected, propane conversion is quite linear as a function of contact time. Figure 1 reports the variations of propene and CO_2 selectivity as a function of contact time. The other products detected are quite minor reaction products under those conditions. Since the contact time is very low, propene and CO_2 selectivities are quite equal; as T_c increases up to $T_c = 1.2$ s, CO_2 selectivity decreases rapidly

(propene formation is thus improved). These results obtained at low contact time indicate that propene and CO_2 are both primary products. When T_c is as high as 1.2 s, secondary oxidative reactions occur, and CO_2 selectivity then gradually increases. CO_2 is thus both a primary and a secondary product. While T_c is as high as 6 s, propane conversion increases to 5%, and CO_2 selectivity seems to stabilize, in relation to the appearance of quite high CO selectivity as already reported above.

Performances of $AgMo_3P_2O_{14}$ were also studied under more oxidative conditions ($O_2/C_3H_8 = 1.6$, with a W/F of $3.5\ g \cdot h \cdot liter^{-1}$. The conversion is increased to 8% at 483 K versus 7% for $O_2/C_3H_8 = 1/3$ whereas propene selectivity is lower, 55% versus 70% under reductive conditions. The balance is CO_x selectivity (indeed, acrolein selectivity remains 6%, whatever the temperature). When the O_2/C_3H_8 value is increased even more ($O_2/C_3H_8 = 10$), no more propane conversion is observed whatever the temperature.

Comparison with $AgMoPO_6$, $AgMo_5P_8O_{33}$, $NaMo_5P_8O_{33}$, and $Ag_{0.5}Na_{0.5}Mo_5P_8O_{33}$

In order to explain the differences in activity and selectivity for propane mild oxidation of these two isotypic compounds, the influence of their structural differences, on the catalytic properties, i.e., the nature of the intercalated cation and the molybdenum average oxidation state (see below), was studied. In fact, on the one hand, many systems involving silver are reported to be active (2), and on the other hand, a convenient equilibrium between the Mo^V and Mo^{VI} species could also be fundamental for good catalytic performances. Complementary catalytic tests have thus been performed on $AgMo^{VI}PO_6$, and on three compositions of the solid solution of formulation $Ag_xNa_{1-x}Mo^V_5P_8O_{33}$ ($x = 0$, 0.5, 1) to try to evaluate the role of the silver cation separately from the role of the molybdenum oxidation state. Table 3 summarizes the main results in terms of C_3H_8 conversion and selectivities which were obtained on the six samples at 733 K. It appears that the four other Ag samples are much less active in propane oxidation than the $AMo_3P_2O_{14}$ samples, $AgMoPO_6$ being completely inactive under the test conditions used. As far as the solid solution compounds are concerned, the lower the silver content, the lower the activity, the selectivity in propene being almost constant. It can be noted that the conditions of isoconversion of propane of about 3% correspond to 683 and 733 K, respectively, for $AgMo_3P_2O_{14}$ and $AgMo_5P_8O_{33}$ samples; the propene selectivities are thus of the same order (81%), the acrolein selectivities being slightly higher in the case of $AgMo_5P_8O_{33}$.

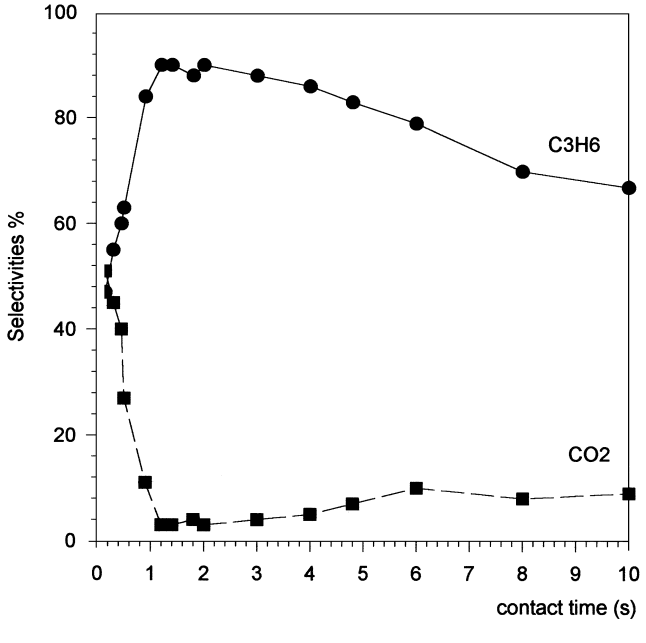

FIG. 1. Study of $AgMo_3P_2O_{14}$ catalyst as a function of contact time: propene and CO_2 selectivities.

TABLE 3

Comparison of Catalytic Results Obtained on Five Samples for Propane Mild Oxidation at 733 K

Compound	Propane conversion (%)	Propene selectivity (%)	Acrolein selectivity (%)	CO_x selectivity (%)
$AgMo_3P_2O_{14}$	7	70	6	18
$SrMo_3P_2O_{14}$	11.5	35	2	59
$AgMo_5P_8O_{33}$	3.5	81	7.5	7
$Ag_{0.5}Na_{0.5}Mo_5P_8O_{33}$	1	85	5	4
$NaMo_5P_8O_{33}$	0.5	86	6	3
$AgMoPO_6$	0	/	/	/

Characterization Results

XRD Results

The crystalline structures of the different compounds have been described separately elsewhere (23–25). Nevertheless, a comparison of their structural features must be presented to allow structure–activity results to be discussed.

First, the six samples studied correspond to three different host lattices: $[MoPO_6]_\infty$ (Fig. 2), $[Mo_5P_8O_{33}]_\infty$ (Fig. 3), and $[Mo_3P_2O_{14}]_\infty$ (Fig. 4). In these three frameworks, molybdenum species exhibit different oxidation states and surroundings. In the $[MoPO_6]_\infty$ framework, the molybdenum atoms are Mo^{VI} species and are located in isolated octahedra, whose geometry corresponds to classical isolated $Mo^{VI}O_6$ octahedra (two "free" molybdenyl bonds). In the $[Mo_5P_8O_{33}]_\infty$ host lattice, molybdenum atoms are pentavalent species and are located in two kinds to Mo^VO_6 octahedra: the first one corresponds to isolated octahedra with its classical characteristics (32), i.e., one "free"

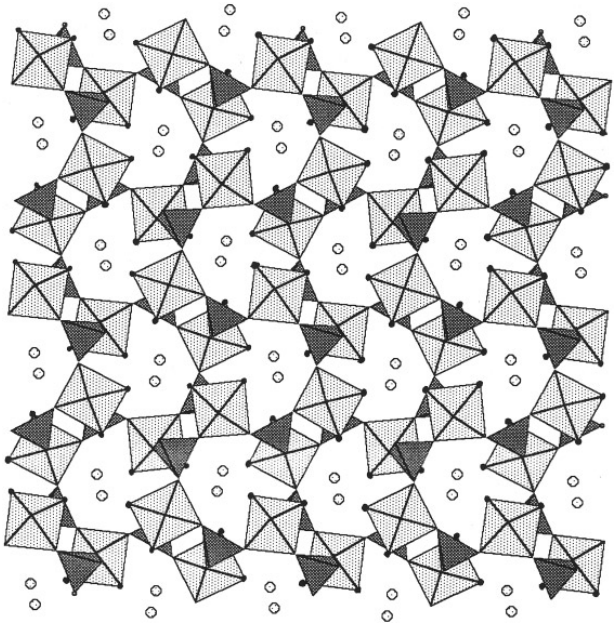

FIG. 2. Projection of $AgMoPO_6$ along [001] (dark circles at the apex of MoO_6 octahedra mark oxygen of molybdenyl bonds).

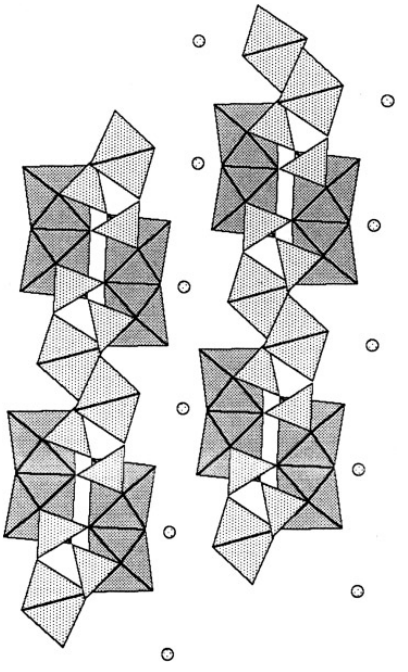

FIG. 4. Projection of $AMo_3P_2O_{14}$ structure along [010].

molybdenyl bond; the second one is involved in infinite $(MoO_3)_\infty$ chains, once more with one short molybdenyl bond, but a "linked" one, in this case. The latter is involved in the O=Mo $\cdots$ O bridge [the molybdenyl bond (≈1.65 Å) is represented here and in the following text by Mo=O to differentiate it from the long *trans*-molybdenyl bond, represented as Mo $\cdots$ O (≈2.3 Å), and from the equatorial bond (≈2 Å)]. In $[Mo_3P_2O_{14}]_\infty$, the Mo atoms are located on three independent crystallographic sites and their relative positions lead to an Mo_3O_{15} unit which is composed of two octahedra linked by one edge and one trigonal bipyramid linked to one of the two octahedra by one corner. The exact geometry of this unit is described in Fig. 5 for $AgMo_3P_2O_{14}$. In this case, the average molybdenum oxidation state is 5.66, the mixed valency being a localized one with the repartition $(Mo^V)_{oct}(Mo^{VI})_{oct}(Mo^{VI})_{bipyr}$ in the Mo_3O_{15} unit (23). When strontium (divalent cation) in substituted for silver (monovalent cation), the average molybdenum oxidation state becomes 5.33 with the new repartition $(Mo^V)_{oct}(Mo^V)_{oct}(Mo^{VI})_{bipyr}$ (23). These valency localizations have been obtained from electrostatic

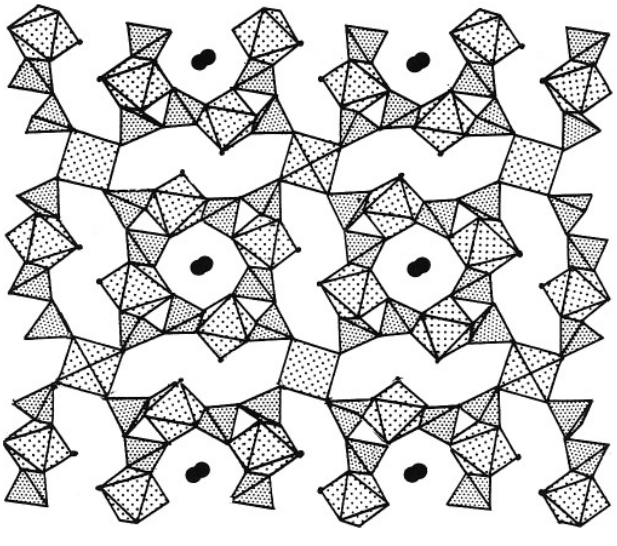

FIG. 3. Projection of $AgMo_5P_8O_{33}$ along [100] (dark circles at the apex of MoO_6 octahedra mark oxygen of molybdenyl bonds).

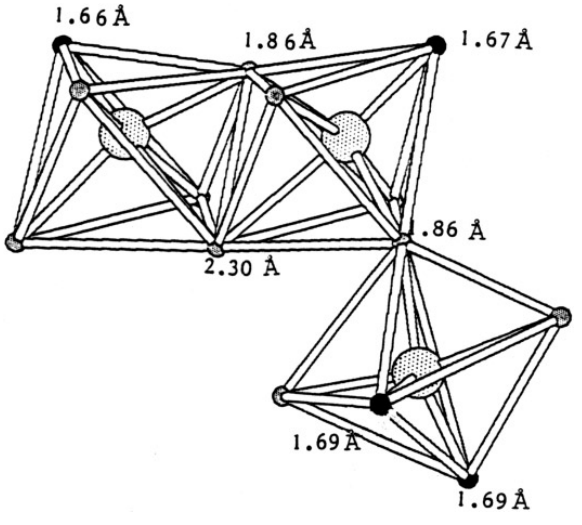

FIG. 5. Mo_3O_{15} unit in $AgMo_3P_2O_{14}$.

TABLE 4

Geometry of the Central Octahedron in Mo_3O_{15} Units in $AgMo_3P_2O_{14}$ and $SrMo_3P_2O_{14}$

$AgMo_3P_2O_{14}$: MoO bonds (Å) in $Mo^{VI}O_6$	$SrMo_3P_2O_{14}$: MoO bonds (Å) in $Mo^{V}O_6$
1.865	1.92
2.302	2.33
1.673	1.63
1.866	1.97
2.002	2.06
2.002	2.06

valency calculations (33). Note that the MoO bonds of the central octahedron are slightly different as a function of the oxidation state of the Mo atom (Table 4): in the $Mo^{V}O_6$ central octahedron of $SrMo_3P_2O_{14}$, the molybdenyl bond is shorter and the five other bonds are longer than those in the $Mo^{VI}O_6$ central octahedron of $AgMo_3P_2O_{14}$. These geometric data are in agreement with results obtained on isolated octahedra (32).

As far as cations are concerned, three kinds of situations must be considered. In the $[MoPO_6]_\infty$ framework, silver cations are blocked inside windows delimited by the host lattice, the "free" oxygen atoms (molybdenyl bonds) of each $Mo^{VI}O_6$ octahedron, which are represented by dark circles in Fig. 2, participate quite strongly in the coordination of the silver cations (≈2.37–2.72 Å). In $AgMo_5P_8O_{33}$, silver cations are located inside large tunnels (Fig. 3), and they exhibit very high thermal factors ($B_{eq} = 4$–6 Å^2). These high values can be related to the fact that, in contrast to the case of the previous compound, the oxygen atoms of the free molybdenyl bonds of the framework, which are also marked by dark circles in Fig. 3, do not participate in the coordination of the silver atoms and do not allow them to be strongly stabilized (Ag–O distances ranging from (2.35 to 2.282 Å) Lii and co-workers (25) suggested that, due to the low stabilization of the inserted cation, this framework could, possess some ionic conduction properties. Nevertheless, technical problems do not yet allow verification of this physical property. When sodium is progressively substituted for silver, no ordering phenomena are found, so we can consider that there is a random repartition of all the cations on silver crystallographic sites. The $[Mo_3P_2O_{14}]_\infty$ host lattice is a layer structure; the cations (silver or strontium) are thus intercalated between the $[Mo_3P_2O_{14}]_\infty$ layers (Fig. 3). This can make possible the displacement of the cations between the layers.

XANES Results

The Mo *K*-edges of molybdenum metal and of some oxides used as references for Mo(0), Mo(V) (34), Mo(5.33) (35), and Mo(VI) (36) valence states and the $AgMo_3P_2O_{14}$ before [Mo(5.66) (23)] and after catalytic test are shown in Fig. 6. The edge energies for each compound have been measured on the derivative spectra and correspond to mid-height of the main absorption jump: they are reported in Table 5. From the edge energies of the reference spectra for Mo(V) [$NaMo_3P_2O_{13}$ (34)] and Mo(5.66) ($AgMo_3P_2O_{14}$ before catalytic test) and assuming a linear dependence of the edge energies on the mean formal valence state of molybdenum cations, an estimation of the Mo valency is proposed for the $AgMo_3P_2O_{14}$ compound after catalytic test (Table 5) which indicates clearly that a random of molybdenum from

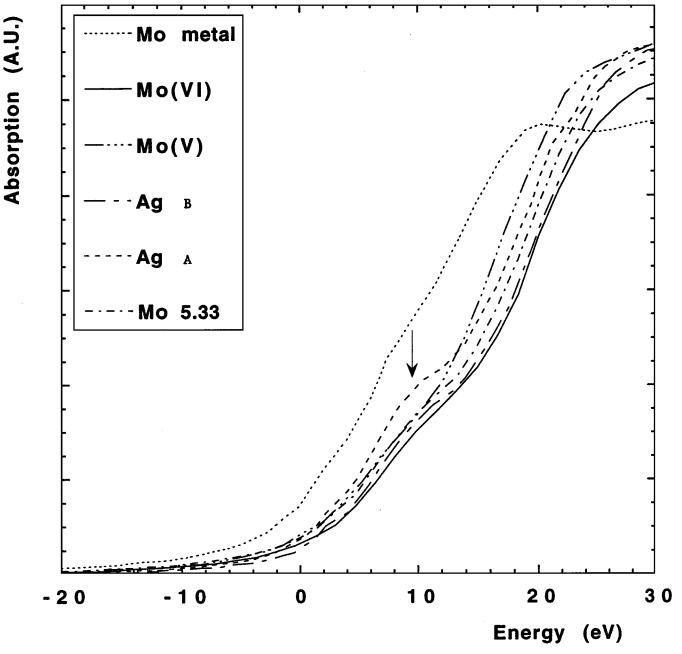

FIG. 6. XANES, Mo *K*-edge of molybdenum phosphate references involving different Mo valencies: Mo^0 metal, Mo^{V} $NaMo_3P_2O_{13}$, $Mo^{5.33}$ $NaMo_3P_6O_{16}$, Mo^{VI} $BaMo_2P_2O_{12}$, and $AgMo_3P_2O_{14}$ before (B) and after (A) catalytic test.

TABLE 5

Mo Valencies Estimated from Mo *K*-Edge Energies

Compound	Mo formal valence state	Energy (eV) at midheight of the main jump	Estimated formal valence state
Mo metal	Mo(0)	11.2 ± 0.3	
$NaMo_3P_2O_{13}$	Mo(5)[a]	15.4 ± 0.3	
$NaMo_3P_6O_{16}$	Mo(5.33)	17.2 ± 0.3	5.45 ± 0.3
$BaMo_2P_2O_{12}$	Mo(6)	18.6 ± 0.3	5.80 ± 0.3
$AgMo_3P_2O_{14}$ (B)	Mo(5.66)[a]	18.1 ± 0.3	
$AgMo_3P_2O_{14}$ (A)		16.4 ± 0.3	5.25 ± 0.3

Note. (B) Before catalytic test; (A) after catalytic test.

[a] Theoretical formal valence state deduced from the crystallographic data and assuming the oxygen stoichiometry given above.

5.66 to 5.25 occurs during the catalytic process. The structural changes involved in such a reduction will be described more precisely in the EXAFS paragraph.

An important indication of the local structural changes involved in the catalytic process can be obtained from the variation in intensity of the prepeak marked by an arrow in Fig. 6. The prepeak arises from an electronic transition from the Mo(1*s*) core level to the hybridized Mo($4d_{t2g}$)–O(2*p*)–Mo(5*p*) molecular orbitals, allowing insight into the 4*d* orbitals to be gained at the Mo *K*-edge, although the $1s \rightarrow 4d$ transition is dipolar forbidden. The prepeak intensity is directly linked to the degree of hybridization of the Mo(4*d*) and O(2*p*) orbitals; this hybridization increases with the distortion of the MoO_6 octahedron and more precisely with the deviation of the molybdenum position with respect to the center of symmetry of the octahedron. The strong increase of the prepeak intensity on the Mo *K*-edge of the $AgMo_3P_2O_{14}$ compound after the catalytic test (Fig. 5) is a clear indication of a strong increase in the MoO_6 octahedron distortion which is linked to the molybdenum reduction.

EXAFS Results

The local bonding around the molybdenum center was examined using the EXAFS technique, above the molybdenum X-ray absorption threshold. The moduli of the Fourier transforms of the experimental EXAFS spectra of $AgMo_3P_2O_{14}$ before and after catalytic tests are shown in Fig. 7.

All peaks are shifted to radii shortened by 0.35 Å owing to the presence of a backscattering phase shift. When theoretical backscattering phase shifts and amplitudes are included in the calculation of model spectra, the positional agreement between the calculated model structure and the experimental data is quite good. As far as the oxygen shell is concerned, two kinds of peaks can be considered: those corresponding to molybdenyl short bonds and those corresponding to the longer Mo–O bonds. Therefore, the fits performed between 3 and 13.2 $Å^{-1}$ on $k\chi(k)$ EXAFS spectra from a back-Fourier transform taken from 1 to 2.2 Å took into account two separate layers corresponding to the oxygen short Mo=O layer and to the Mo–O (≈2 Å) layer. These two layers are respectively characterized by (N_1–R_1, N_2–R_2) parameters (N–R = number of O atoms and MoO average distance of one layer). Taking into account that the amplitude and phase shift are theoretical files, we took $\Gamma = 1$ and $S_0 = 0.8$, and then the other parameters were refined.

$AgMo_3P_2O_{14}$ before catalytic test. The (N_1–R_1, N_2–R_2) values are consistent with the (N_{1cm}–R_{1cm}, N_{2cm}–R_{2cm}) (cm means crystallographic model) values which were calculated from X-ray monocrystal diffraction determination (23) (Table 6). Figure 8a exhibits the simulated and experimental EXAFS spectra. The short Mo=O bond present at 1.72 Å is clearly seen and the peak associated with the longer equatorial Mo–O and with the *trans*-molybdenyl bond is the most intense. The $N_1 + N_2 = 5.63$ value is consistent with the crystallographic model and corresponds to two Mo atoms in octahedral coordination and the third in trigonal bipyramidal coordination as described in Fig. 5. A narrow comparison with the crystallographic model shows that, on the one hand, the N_1 value is higher than N_{1cm} (and $N_2 < N_{2cm}$), and on the other hand, the R_1 value is higher

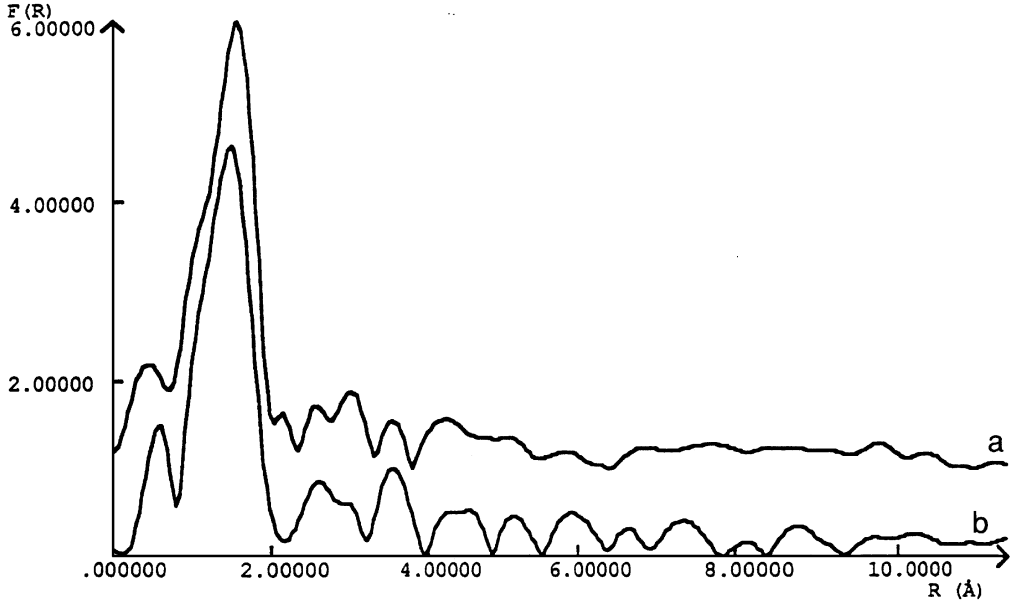

FIG. 7. Fourier transform EXAFS spectra of $AgMo_3P_2O_{14}$ samples: (a) before catalytic test; (b) after catalytic test.

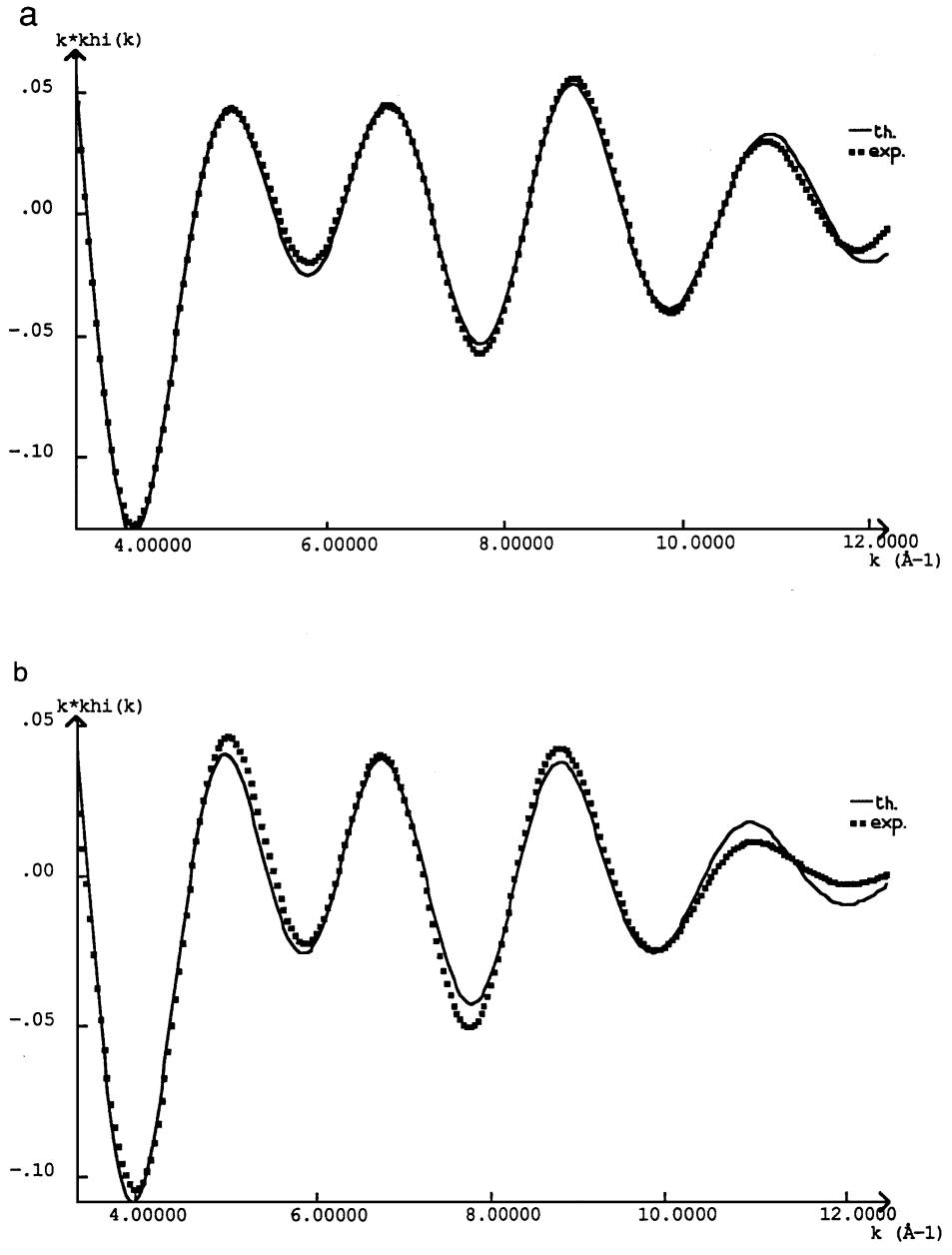

FIG. 8. Simulated and experimental EXAFS spectra of $AgMo_3P_2O_{14}$: (a) before catalytic test; (b) after catalytic test.

than R_{1cm} ($R_2 < R_{2cm}$); this could be related to the difficulty in separating the two oxygen layers experimentally. Indeed, as seen from crystallographic data (Table 4), the two Mo–O distances of 1.86 Å to the central octahedron which have been attributed to the second layer in the crystallographic model could be partly included in the first layer.

$AgMo_3P_2O_{14}$ after catalytic test. First, let us recall some structural results obtained on molybdenum phosphates. It has been shown that Mo^V coordination polyhedra are very specific: one short Mo=O bond (≈1.65 Å), four equatorial Mo–O bonds (≈2 Å), and the long trans-molybdenyl bond (32). As far as Mo^{VI} coordination polyhedra are concerned, until now, two kinds of polyhedra have been known: a trigonal bipyramid with two molybdenyl bonds, and an octahedron with also two molybdenyl bonds (these two bonds are slightly longer (≈1.7 Å) than the bond in the Mo^V octahedra); the other Mo–O bonds are shorter than those in Mo^V octahedra, so that the summation of electrostatic valences (33) leads to a valence of VI for the molybdenum species concerned.

After the catalytic test (Fig. 8b, Table 6), the $(N_1 + N_2)$ value is increased to 6. Moreover, the N_1 and R_1 values have decreased whereas N_2 and R_2 have increased. As seen

TABLE 6

Variation of the EXAFS Parameters before and after Catalytic Test for $AgMo_3P_2O_{14}$: Comparison with the Initial Crystallographic Model Results

	First oxygen layer	Second oxygen layer
Crystallographic model	$N_{1cm} = 1.33$ $R_{1cm} = 1.682(4)$ Å	$N_{2cm} = 4.33$ $R_{2cm} = 2.018(5)$ Å
$AgMo_3P_2O_{14}$ EXAFS parameters before catalytic test	$N_1 = 1.39$ $R_1 = 1.72(1)$ Å $\sigma_1 = 4.72 \times 10^{-2}$ $\tau_1 = 1$ $\Delta E_1 = 6.34$ eV	$N_2 = 4.24$ $R_2 = 2.00(1)$ Å $\sigma_2 = 4.57 \times 10^{-2}$ $\tau_2 = 1$ $\Delta E_2 = 3.00$ eV
$AgMo_3P_2O_{14}$ EXAFS parameters after catalytic test	$N_1 = 1.12$ $R_1 = 1.68(1)$ Å $\sigma_1 = 4.57 \times 10^{-2}$ $\tau_1 = 1$ $\Delta E_1 = 3.00$ eV	$N_2 = 4.90$ $R_2 = 2.02(1)$ Å $\sigma_2 = 4.57 \times 10^{-2}$ $\tau_2 = 1$ $\Delta E_2 = 8.26$ eV

above, the decrease of the R_1 value seems to indicate an increase of molybdenum V species in the molybdenum cluster. The variation of the N_1 value confirms this result. Nevertheless, when the molybdenum cluster exhibits only Mo^V species in octahedral coordination, N_1 and N_2 values should be 1 and 5, respectively. On the other hand, the hypothesis of two Mo^VO_6 octahedra (linked by the octahedra edge), the third one being $Mo^{VI}O_6$, would lead to $N_1 = 1.33$, $N_2 = 4.66$. The experimental values are intermediate between these two solutions. In fact, as seen from XANES Mo *K*-edge results (Table 5), after the catalytic test, the average Mo oxidation state is about 5.25, which corresponds to three Mo species clusters with two Mo^V and one $Mo^{V/VI}$ species. This result is in agreement with the global reduction of the sample as seen from R_1, N_1, and N_2 value variations.

XPS Results

$AgMo_3P_2O_{14}$ was analyzed by XPS. It was studied before and after catalytic tests performed at 723 and 623 K. In this latter case, the catalyst presents no activity. After the test, the catalyst was quickly cooled down under argon atmosphere to minimize any structural evolution under air.

Relative surface concentration. The surface atomic ratios are presented in Table 7. The values corresponding to bulk composition determined by chemical analysis are noted in parentheses. After the catalytic test performed at 623 K (low propane conversion), surface concentrations stay very close to those measured before the reaction. Conversely, after the reaction performed at 723 K, some changes are observed. We note an increase in Ag and P concentrations of, respectively, 15 and 13% compared to the initial values. Because the material was prepared at higher temperature (873 K) and was stable under inert atmosphere at the temperature of the catalytic reaction, it can be shown that modifications on the catalyst occur only when the reaction occurs.

TABLE 7

Relative Surface Concentration Measured by XPS

	Mo/Ag	Mo/P	P/Ag
Before catalytic test	2.79(3)	1.22(1.5)	2.27(2)
After catalytic test			
$T_R = 623$ K	2.79	1.17	2.38
$T_R = 723$ K	2.36	1.06	2.22

Surface oxidation state of molybdenum. In order to specify the effect of the reaction on the oxidation state of molybdenum species, the Mo peaks were decomposed into components characterizing $Mo3d_{5/2}$ and $Mo3d_{3/2}$ in the V and VI oxidation states. The samples $AgMo_5P_8O_{33}$ and MoO_3, which present only one oxidation degree of Mo, respectively V and VI, were used as reference compounds. Their $Mo3d_{5/2}$ and $Mo3d_{3/2}$ peaks were fitted. For these reference compounds, the best fits were obtained using Lorentzian curves with parameters such as:

—For $AgMo_5P_8O_{33}$ (Fig. 9):

$Mo3d_{5/2}$, $E_1 = 231.7$ eV; FWHM = 1.5 eV
$Mo3d_{3/2}$, $E_1 = 234.9$ eV; FWHM = 1.5 eV.

—For MoO_3:

$Mo3d_{5/2}$, $E_1 = 232.6$ eV; FWHM = 1.3 eV
$Mo3d_{3/2}$, $E_1 = 235.7$ eV; FWHM = 1.3 eV.

The parameters obtained for these two compounds (binding energy, FWHM, shape) were used to analyze the molybdenum peaks of the mixed valency sample. The decomposition of the peaks of $AgMo_3P_2O_{14}$ before reaction is presented in Fig. 10. The measurement of the area of the $Mo3d_{5/2}$ peaks corresponding to Mo(V) and Mo(VI) allows us to calculate the average oxidation degree of surface Mo. The value obtained (5.57) is in very good agreement with the bulk value (5.66). The spectrum of the same compound after the catalytic test performed at 723 K shows an increase in the contribution of the Mo(V) peak (Fig. 11). In this case, the surface Mo average oxidation degree is 5.34.

DISCUSSION

The different catalytic performance of $AgMo_3P_2O_{14}$ and $SrMo_3P_2O_{14}$ can be explained by taking into account the molybdenum oxidation state and the nature of the cations.

Evaluation of catalytic properties of other molybdenum phosphates showed that the silver cation may act positively when the organization of the host lattice allows silver migration. Indeed, it appears that, among the three frameworks $[Mo_3P_2O_{14}]_\infty$, $[Mo_5P_8O_{33}]_\infty$, and $[MoPO_6]_\infty$, only the first one enhances both cation migration (in relation to its layer

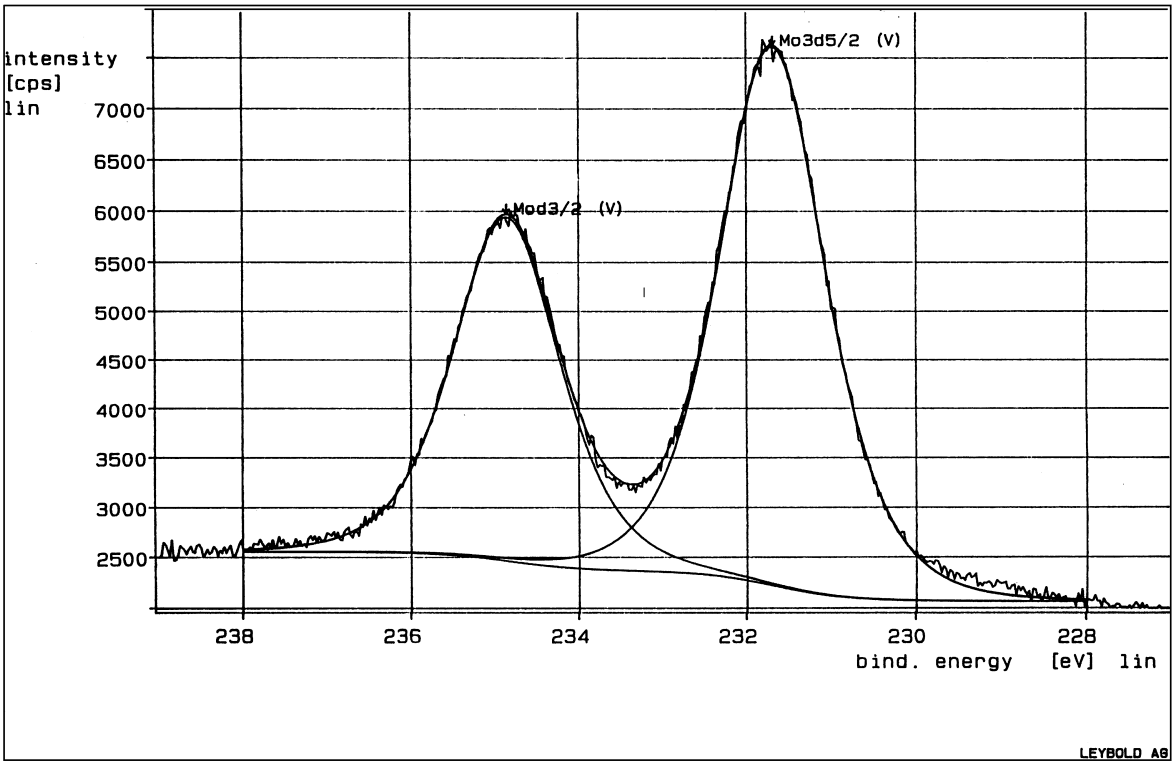

FIG. 9. XPS spectrum of the Mo3*d* peaks of $AgMo_5P_8O_{33}$.

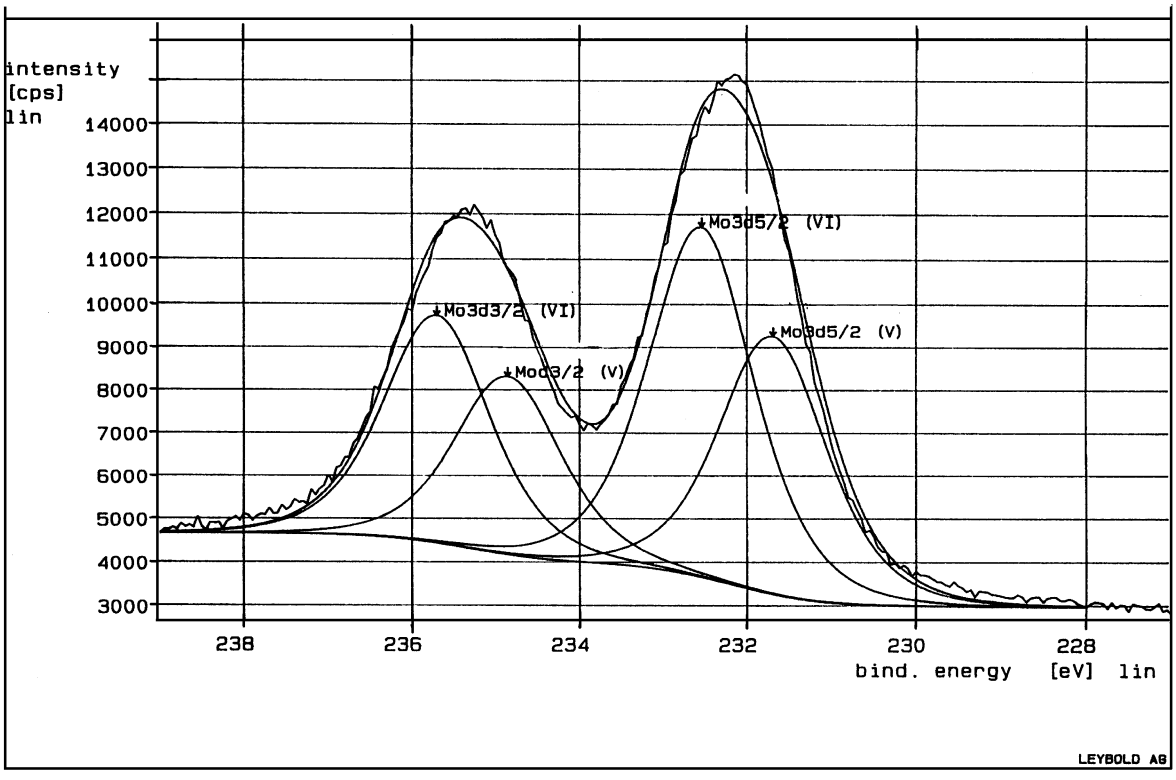

FIG. 10. XPS spectrum of the Mo3*d* peaks of $AgMo_3P_2O_{14}$ before reaction.

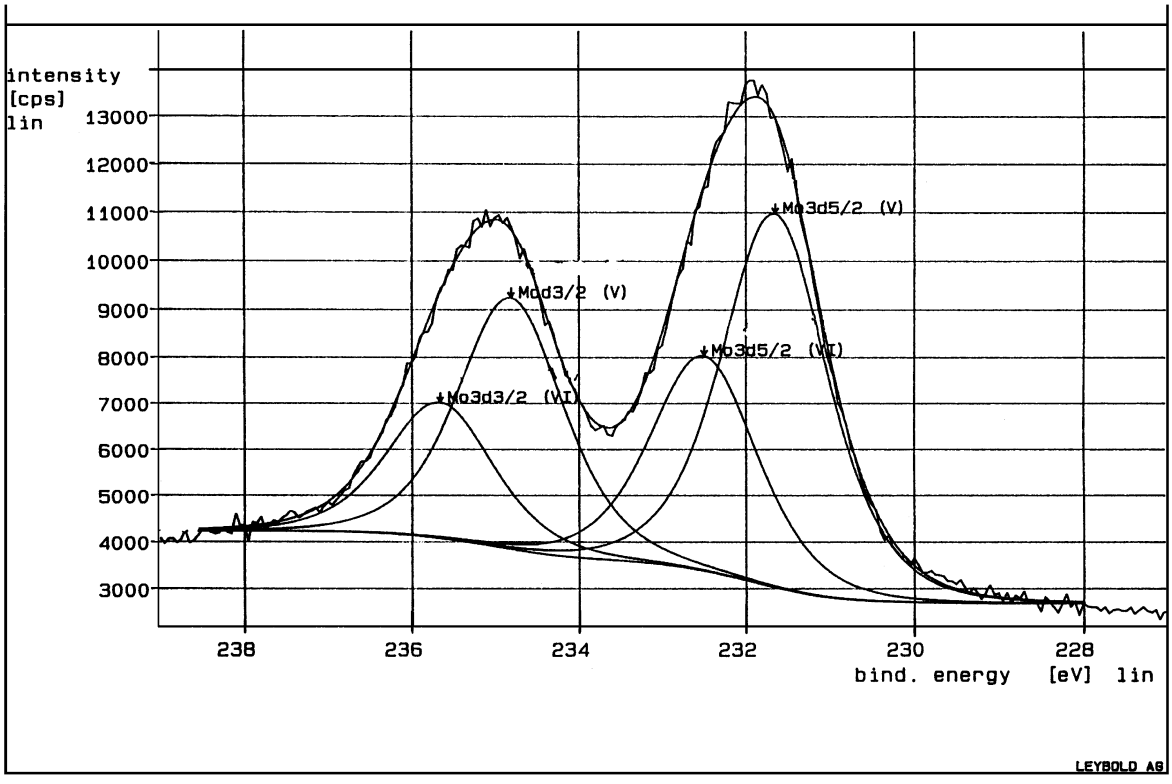

FIG. 11. XPS spectrum of the Mo3*d* peaks of $AgMo_3P_2O_{14}$ after reaction at 723 K.

structure) and electronic exchanges inside Mo_3O_{15} units. This last point must be particularly noted because such electronic exchanges are supposed to occur in redox mechanism reactions. As far as the $[Mo_5P_8O_{33}]_\infty$ framework is concerned, if the existence of large tunnels could allow cation migration, the organization of MoO_6 octahedra would certainly be less favorable than in the previous case because of the presence of isolated octahedra and of infinite $(MoO_3)_\infty$ chains instead of limited polynuclear clusters as Mo_3O_{15} units. These structural particularities result in a lower activity of this host lattice than of the $[Mo_3P_2O_{14}]_\infty$ lattice, but the positive influence of silver could nevertheless clearly be shown in this example. The last $[MoPO_6]_\infty$ framework exhibits only isolated octahedra and, moreover, it does not allow cations to move.

It can be concluded that the main structural criterion for obtaining a good catalytic result in mild propane oxidation concerns the nature of the host lattice and, in particular, the situation of Mo atoms relative to each other. Polynuclear transition metal clusters of limited size seem to enhance electronic exchanges, and the presence of double bridges

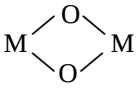

in these clusters, already seen in vanadyl pyrophosphate $(VO)_2P_2O_7$, which is active for *n*-butane oxidation reaction (37), is certainly favorable. The influence of cations also occurs, but it is largely related to the framework, which can inhibit or promote its effect.

Even if, as shown by XRD characterization, no deep modification of the $AgMo_3P_2O_{14}$ catalyst occurred during the reaction, other complementary characterizations used in the present study show that the catalyst is slightly modified during the catalytic test. Let us remember here that the host lattice $[Mo_3P_2O_{14}]_\infty$ is stabilized by mono- or divalent cations, which involves the central octahedra containing a Mo^{VI} or Mo^{V} atom, respectively, and indicates a large flexibility of the framework, which can accept various oxidation states without strong geometrical modifications.

The main result obtained by XANES and confirmed by EXAFS spectra concerns the partial reduction of the average molybdenum oxidation state in $AgMo_3P_2O_{14}$ from 5.66 before catalytic test to 5.25 after reaction. Comparison of surface (XPS) and bulk characterizations showed good agreement between the molybdenum oxidation states measured by the two techniques. This indicates that the modification of the catalyst affects the whole volume and not only the first layers. This kind of result has already been seen in oxidation catalysis. For example, isotopic exchanges performed with ^{18}O proved the participation of the oxygen atoms of the whole catalyst lattice in the oxidation reaction (38). If we consider the molybdenum average oxidation state of 5.25 found for $AgMo_3P_2O_{14}$ after the reaction,

we could explain the better activity of the strontium isotypic compound by its initial quite good balance between the Mo^{V} and Mo^{VI} species ($Mo^{5.33}$). Moreover, the total inactivity of $AgMo_3P_2O_{14}$ over a very oxidative atmosphere ($O_2/C_3H_8 = 10$) (the required 2/1 Mo^{V}/Mo^{VI} equilibrium can not be achieved in such an oxidative atmosphere) indicates once more the importance of the establishment of a convenient redox equilibrium. As far as $AgMo_3P_2O_{14}$ is concerned, and considering the Mo_3O_{15} units described in Fig. 5, we can propose a structural model (after catalytic reaction performed under reductive conditions) based on absorption X-ray results. First, the reduction of the molybdenum state from 5.66 to 5.25 should result in a different distribution of Mo^{V} and Mo^{VI} species in this unit. We must recall here that the molybdenum atom of the central octahedron of the Mo_3O_{15} unit has been found to be either Mo^{V} or Mo^{VI} according to the valence of the intercalated cation. It could therefore be considered that at least part of the observed reduction ($Mo^{5.66} \rightarrow Mo^{5.33}$) corresponds to the reduction of this central molybdenum in the Mo_3O_{15} unit. This modification should result in a shortening of the average molybdenyl bonds. This is effectively observed in the first oxygen shell considered by EXAFS ($R_1 = 172$ Å $\rightarrow$ $R_1 = 168$ Å).

To explain the increase of the molybdenum coordination number ($N_1 + N_2 = 5.63 \rightarrow N_1 + N_2 = 6$), the decrease of molybdenyl bonds ($N_1 = 1.33 \rightarrow N_1 = 1.1$), and the molybdenum oxidation state, which is slightly lower (5.25) than that expected from the above considerations (5.33), the third molybdenum atom environment, whose coordination polyhedron initially is a trigonal bipyramid, must be taken into account. Three hypotheses must be considered.

The trigonal bipyramidal coordination of this atom may be transformed into octahedral coordination ($N_1 + N_2 = 5.63 \rightarrow N_1 + N_2 = 6$). The apparent paradox between a larger coordination number and a more reduced state can be overcome by involving different bond lengths. Moreover, the increase in the molybdenum coordination number does not necessarily imply an increase in the number of oxygen atoms in the host lattice: for example, the new octahedron can share one edge with the central one, since the EXAFS technique does not give any information about the position of the third octahedron in comparison with the others. Nevertheless, due to the global reduction of the MoPO lattice, the problem of electroneutrality of the structure must be considered. As far as the surface is concerned, the increase of its silver composition observed by XPS could compensate the ionic deficit. However, such a feature would not be convenient with the global participation of the whole framework.

The increase in oxygen atom neighbors close to molybdenum atoms could also be due to the presence of water molecules in the environment of the third molybdenum atom, inside the framework. Indeed, water is produced in the oxidation reaction, and the layer structure could quite easily stabilize the water molecule. If the eventual departure of some oxygen species to compensate for the partial reduction of molybdenum atoms in the framework would be in contradiction with the $N_1 + N_2$ increase to 6, the replacement of one oxygen of the molybdenyl ions of the trigonal bipyramid by one hydroxyl group should be considered.

The phosphorus enrichment on the surface observed by XPS measurements has already been seen in VPO systems in butane oxidation (39, 40). The excess of phosphorus at the surface was thus said to stabilize the active phase $(VO)_2P_2O_7$. Such stabilization could also occur in the present case: the active sites described above as trinuclear molybdenum clusters are isolated from each other by phosphorus atoms. This isolation of active sites performed by phosphorus species could thus avoid deeper oxidation, as already suggested by Centi (41).

As far as the role of silver cations is concerned, the increase in their concentration at the surface could be interpreted as evidence of silver displacements occurring during the catalytic reaction. This cationic migration could participate in electronic exchange mechanisms related to molybdenum reduction. Many investigations have revealed that the lattice oxygen ions are incorporated into the oxidation products in several complex oxides (38, 42), suggesting that good catalytic activity involves good participation of the oxygen lattice in the oxidation. In order to verify the participation of the oxygen lattice in the oxidation mechanism, experiments without oxygen in the flow were performed: low propane conversion was thus obtained and acrolein formation was even detected in the first minutes of the reaction. We could therefore consider that one of the roles of the silver cation is to accelerate, by its movements inside the host lattice, the diffusion of bulk oxygen ions (the labile oxygen species are certainly those involved in molybdenyl bonds) and to maintain a high activity of oxygen on the catalyst surface. This interpretation considers the catalyst to be a dynamic system. An EXAFS *in situ* study at the Mo and Ag edges is in progress and should help to clarify the role of silver in the reaction mechanism.

CONCLUSION

A new silver molybdenum phosphate, $AgMo_3P_2O_{14}$, was found to play a role in propane oxydehydrogenation (6% propane conversion, 70% propene selectivity at 733 K). The isotypic $SrMo_3P_2O_{14}$ compound is even more active (12% of propane conversion at 733 K), but less selective in propene. Even if they both present structural units which seem to act favorably in this kind of reaction (Mo_3O_{15} unit and a mixed valency Mo^{V}/Mo^{VI}), other properties must be involved to explain their different catalytic performances such as the initial balance between the Mo^{V} and Mo^{VI} species: the best

equilibrium between these two species seems to be about $Mo^{V}/Mo^{VI} \approx 2/1$, which corresponds to the initial and final distributions in the strontium and silver compounds, respectively. The presence of silver as cation seems to have a good influence on the behavior of the catalyst during the reaction. XPS and X-ray absorption spectroscopy show that silver cations migrate toward the surface during the reaction. This movement induces electronic exchanges particularly in the Mo_3O_{15} units, which are partially reduced after the catalytic reaction ($5.66 \rightarrow 5.25$). The silver species would then stabilize the active phase and facilitate a kind of "breathing" of the catalyst during the catalytic reaction.

REFERENCES

1. Kim, Y. C., Ueda, W., and Moro-Oka, Y., *Appl. Catal.* **70**, 175 (1991).
2. Kim, Y. C., Ueda, W., and Moro-Oka, Y., *in* "New Developments in Selective Oxidation" (G. Centi and F. Trifiro, Eds.), p. 491. Elsevier, Amsterdam, 1990.
3. Kim, Y. C., Ueda, W., and Moro-Oka, Y., *Catal. Today* **13**, 673 (1992).
4. Conner, W. C., Jr., Soled, S., and Signorelli, A., *Stud. Surf. Sci. Catal.* **7**, 1224 (1991).
5. Komatsu, T., Uragami, Y., and Otsuka, K., *Chem. Lett.*, 1903 (1988).
6. Takita, Y., Yamashita, H., and Moritaka, K., *Chem. Lett.*, 1733 (1989).
7. Ai, M., *J. Catal.* **101**, 389 (1986).
8. Ai, M., *Catal. Today* **13**, 679 (1992).
9. Centi, G., Pesheva, D., and Trifiro, F., *Appl. Catal.* **33**, 343 (1987).
10. Centi, G., Grasseli, R. K., Patane, E., and Trifiro F., *in* "New Developments in Selective Oxidation" (G. Centi and F. Trifiro, Eds.), p. 515. Elsevier, Amsterdam, 1990.
11. Centi, G., Grasseli, R. K., and Trifiro, F., *Catal. Today* **13**, 661 (1992).
12. Hodnett, B. K., *Catal. Rev. Sci. Eng.* **27**, 373 (1985).
13. Centi, G., and Trifiro, F., *Chem. Rev.* **88**, 55 (1988).
14. Cavani, F., and Trifiro, F., *Chem. Tech.*, 18 (1994).
15. Bhattacharayya, D., Bey, S. K., and Rao, M. S., *Appl. Catal. A* **87**, 29 (1992).
16. Chaar, M. A., Patel, D., and Kung, H. H., *J. Catal.* **109**, 463 (1988).
17. Siew Hew Sam, D., Soenen, V., and Volta, J. C., *J. Catal.* **123**, 417 (1990).
18. Smits, R. H. H., Seshan, K., and Ross, J. R. H., *Stud. Surf. Sci. Catal.* **72**, 221 (1992).
19. Cherrak, A., Hubaut, R., Barbaux, Y., and Mairesse, G., *Catal. Lett.* **15**, 377 (1992).
20. Mazzochia, C., Aboumard, C., Diagne, D., Temesti, E., Hermann, J. M., and Thomas, G., *Catal. Lett.* **10**, 181 (1991).
21. Corma, A., Lopez-Nieto, A., and Paredes, N., *J. Catal.* **144**, 425 (1993).
22. Gao, X., Ruiz, P., Xin, Q., Guo, X., and Delmon, B., *J. Catal.* **148**, 56 (1994).
23. Borel, M. M., Guesdon, A., Leclaire, A., Grandin, A., and Raveau, B., *Z. Allg. Anorg. Chem.* **620**, 569 (1994).
24. Kierkegaard, P., and Holmen, S., *Ark. Kemi.* **23**, 213 (1964).
25. Lii, K. H., Johnston, D. C., Goshorn, D. P., and Haushalter, R. C., *J. Solid. State Chem.* **71**, 131 (1987).
26. Lyttle, F. W., Sayers, D. E., and Stern, E. A., *Phys. Rev. B* **11**, 4825 (1975).
27. Stern, E. A., Sayers, D. E., and Lyttle, F. W., *Phys. Rev. B* **11**, 4836 (1975).
28. Michalowicz, A., Logiciels pour la Chimie, p. 102. Société Française de Chimie, Paris, 1991.
29. Lengeler, B., and Eisenberg, P., *Phys. Rev. B* **21**, 4507 (1980).
30. Teo, B. K., and Lee, P. A., *J. Am. Chem. Soc.* **101**, 2815 (1979).
31. James, F., and Ross, M., MINUIT, CERN Computing Centre Program Library, CERNID Internal Report 75/20 (1976).
32. Costentin, G., Borel, M. M., Grandin, A., Leclaire, A., and Raveau, B., *Rev. Inorg. Chem.* **13**(2), 77 (1993).
33. Zachariasen, W. H., *J. Less-Common Met.* **62**, 1 (1978).
34. Costentin, G., Borel, M. M., Grandin, A., Leclaire, A., and Raveau, B., *J. Solid. State Chem.* **89**, 31 (1990).
35. Costentin, G., Borel, M. M., Grandin, A., Leclaire, A., and Raveau, B., *J. Solid. State Chem.* **95**, 168 (1991).
36. Masse, R., Averbuch-Pouchot, M. T., and Durif, A., *J. Solid. State Chem.* **58**, 157 (1985).
37. Bordes, E., and Courtine, P., *J. Catal.* **57**, 236 (1979).
38. Ueda, W., Moro-Oka, Y., and Ikawa, T., *J. Catal.* **70**, 409 (1981).
39. Cornaglia, L., Caspani, C., and Lombardo, E. A., *Appl. Catal.* **74**, 15 (1991).
40. Batis, N. H., and Batis, H., *Bull. Soc. Chim. Fr.* **130**, 807 (1993).
41. Centi, G., *Catal. Lett.* **22**, 53 (1993).
42. Krenzle, L. D., and Keulks, G. W., *J. Catal.* **61**, 316 (1980).